Cobalt nanoparticle-embedded nitrogen-doped carbon/carbon nanotube frameworks derived from metal-organic framework for tri-functional ORR, OER and HER electrocatalysis

Hele Guo,[a†] Qichun Feng,[a†] Jixin Zhu,[b] Jingsan Xu,[c] Qianqian Li,[a] Siliang Liu,[a] Kaiwen Xu,[a] Chao Zhang*[a] and Tianxi Liu*[a]

[a]State Key Laboratory for Modification of Chemical Fibers and Polymer Materials, College of Materials Science and Engineering, Innovation Center for Textile Science and Technology, Donghua University, Shanghai 201620, P. R. China

[b]Shaanxi Institute of Flexible Electronics (SIFE), Northwestern Polytechnical University (NPU), 127 West Youyi Road, Xi'an 710072, P. R. China

[c]School of Chemistry, Physics and Mechanical Engineering, Queensland University of Technology, Brisbane, QLD 4001, Australia

* E-mail: czhang@dhu.edu.cn (C. Zhang)

* E-mail: txliu@dhu.edu.cn (T. X. Liu)

† These authors contributed equally to this work.

Electronic Supplementary Information

Materials

Cobalt acetate tetrahydrate (98%), adenine (99%) and Pt/C catalysts (20 wt% Pt loading on an activated carbon support) were obtained from Alfa Aesar. *N*,*N*-Dimethylformamide (99.5%, AR) was obtained from Aladdin. All the reagents were used without further purification.

Characterization

The morphology of the samples was evaluated by FESEM (Ultra 55) and TEM (Tecnai G2 20 TWIN). FTIR spectra were taken by a Nicolet Nexus-670 (Nicolet, USA) in the range of 400-4000 cm^{-1}. The elemental analysis was performed by Elementar Vario EL III (Elementar Analysensysteme GmbH, Germany) based on JY/T 017-1996 general rules for elemental analyzer. Nitrogen adsorption/desorption measurements were conducted at -196 °C in a N_2 atmosphere using a Quantachrome Autosorb-iQ-AG porosimeter. The surface area was calculated by applying the Brunauer-Emmett-Teller (BET) model to the isotherm data points of the adsorption branch in the relative pressure range $p/p_0 < 0.3$. The pore size distribution was calculated from nitrogen sorption data using the nonlocal density functional theory (NLDFT) equilibrium model method for slit pores provided by Quantachrome data reduction software ASiQWin Version 4.01.

Electrochemical measurements

ORR:

The K-L equation is applied to investigate the ORR exact kinetic parameters. The K-L equation can be described as follows:

$$\frac{1}{j}=\frac{1}{j_k}+\frac{1}{j_d}=\frac{1}{j_k}+\frac{1}{B\omega^{-\frac{1}{2}}} \quad (1)$$

$$B=0.2nFC_0D_0^{\frac{2}{3}}\vartheta^{-\frac{1}{6}} \quad (2)$$

$$j_k=nFkC_0 \quad (3)$$

where J is the current density, Jk is the kinetic current density, ω is the rotation speed, n is the transferred electron number, F is the Faraday constant (F = 96485 C

mol^{-1}), C_0 is the saturated concentration of oxygen in the electrolyte (1.21×10^{-3} mol L^{-1}), D_0 is the diffusion coefficient of oxygen in the solution (1.9×10^{-5} cm s^{-1}), υ is the kinetic viscosity of the electrolyte (0.01 cm^2 s^{-1}), and k is the electron-transfer rate constant.

Figure captions:

Fig. S1 SEM images of (a, b) Co@N-CNTF-1-600, (c, d) Co@N-CNTF-2-600 and (e, f) Co@N-CNTF-3-600 at low and high magnifications, respectively.

Fig. S2 (a, b) TEM images and (c) corresponding size distributions of Co nanoparticles within the Co@N-CNTF-2-600.

Fig. S3 SEM images of Co@N-CNTF-2-800 at (a) low and (b) high magnifications, respectively.

Fig. S4 (a, b) TEM images and (c) corresponding size distributions of Co nanoparticles within the Co@N-CNTF-2-800.

Fig. S5 XPS survey spectra of the Co@N-CNTF samples.

Fig. S6 (a) Co 2p and (b) N 1s XPS curves of the Co@N-CNTF-2-600, Co@N-CNTF-2-700 and Co@N-CNTF-2-800.

Fig. S7 Atomic contents of nitrogen in the Co@N-CNTF samples

Fig. S8 Atomic contents of various nitrogen forms in the Co@N-CNTF-2-600, Co@N-CNTF-2-700 and Co@N-CNTF-2-800.

Fig. S9 Raman spectra of the Co@N-CNTF-2-600, Co@N-CNTF-2-700 and Co@N-CNTF-2-800.

Fig. S10 XRD patterns of the Co@N-CNTF-2-600, Co@N-CNTF-2-700 and Co@N-CNTF-2-800.

Fig. S11 LSV curves of the Co@N-CNTF-2-600, Co@N-CNTF-2-700 and Co@N-CNTF-2-800 in O_2-saturated 0.1 M KOH at 1600 rpm.

Fig. S12 Tafel slopes of the Co@N-CNTF-1, Co@N-CNTF-2 and Co@N-CNTF-3 in O_2-saturated 0.1 M KOH at 1600 rpm.

Fig. S13 CV plots of (a) Co@N-CNTF-2-600, (b) Co@N-CNTF-1, (c) Co@N-CNTF-2, (d) Co@N-CNTF-3, (e) Co@N-CNTF-2-800 at different scan rates. (f) The measured capacitive currents plotted as a function of scan rates.

Fig. S14 CV curves of Co@N-CNTF-1, Co@N-CNTF-2 and Co@N-CNTF-3 in O_2-saturated 1 M KOH with a sweep rate of 5 mV s^{-1}.

Fig. S15 XRD pattern of the Co@N-CNTF-2-700 after cycling for the OER.

Fig. S16 Raman spectra of the Co@N-CNTF-2-700 after cycling for the OER.

Fig. S17 XPS spectra of the Co@N-CNTF-2-700 after cycling for the OER. (a) XPS survey, (b) Co 2p, (c) O 1s, and (d) C 1s spectra.

Fig. S18 The ORR performance of the Co@N-CNTF-2-700 after cycling for the OER.

Fig. S19 Schematic of a home-made water splitting device using carbon cloth-loaded Co@N-CNTF-2 as both cathode and anode by chronopotentiometry at 10 mA cm^{-2}. (b) The volume of produced H_2 and O_2 as a function of the water-splitting time for the device.

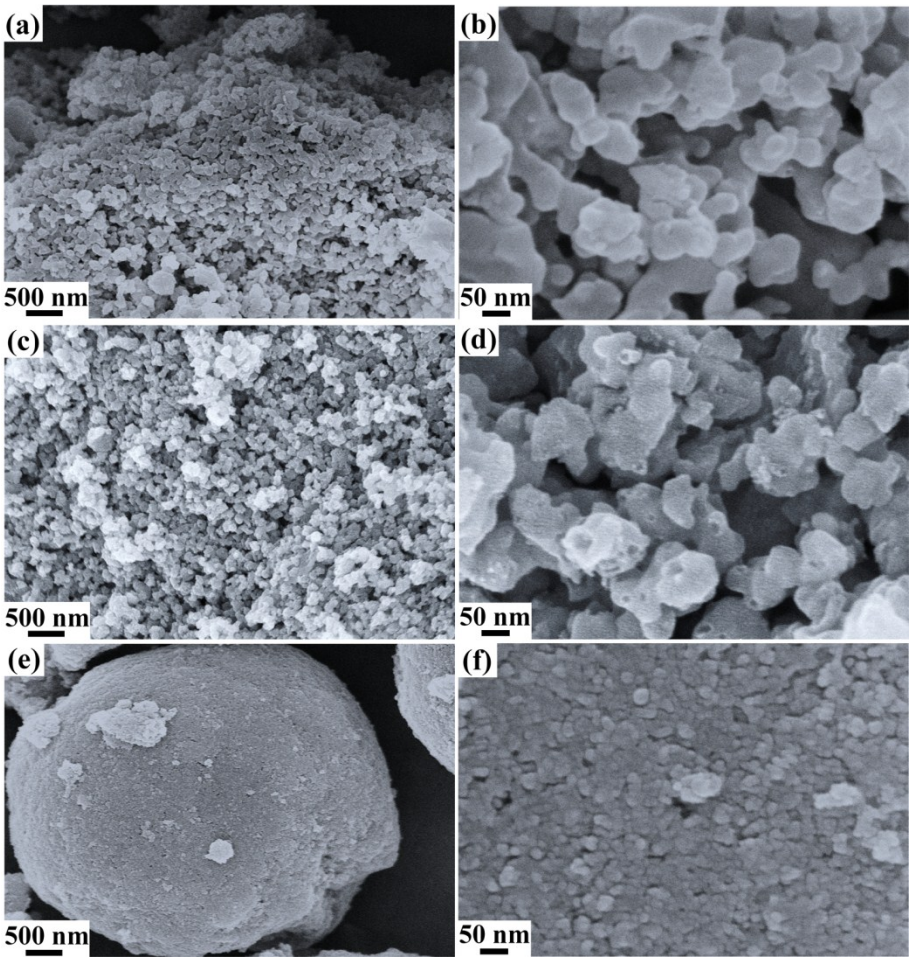

Fig. S1 SEM images of (a, b) Co@N-CNTF-1-600, (c, d) Co@N-CNTF-2-600 and (e, f) Co@N-CNTF-3-600 at low and high magnifications, respectively.

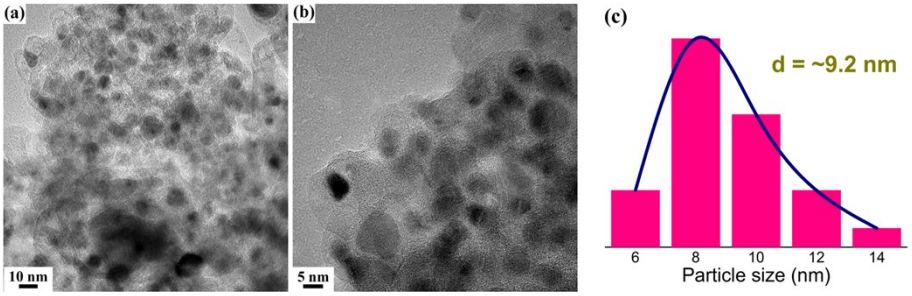

Fig. S2 (a, b) TEM images and (c) corresponding size distributions of Co nanoparticles within the Co@N-CNTF-2-600.

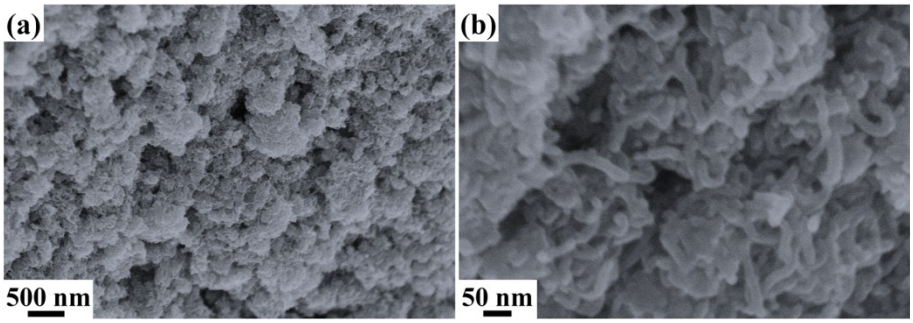

Fig. S3 SEM images of Co@N-CNTF-2-800 at (a) low and (b) high magnifications, respectively.

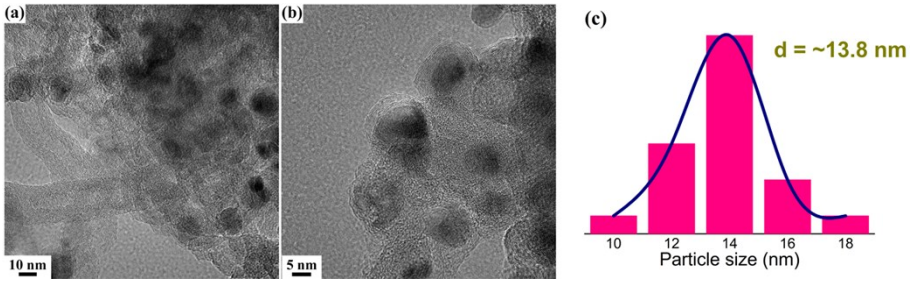

Fig. S4 (a, b) TEM images and (c) corresponding size distributions of Co nanoparticles within the Co@N-CNTF-2-800.

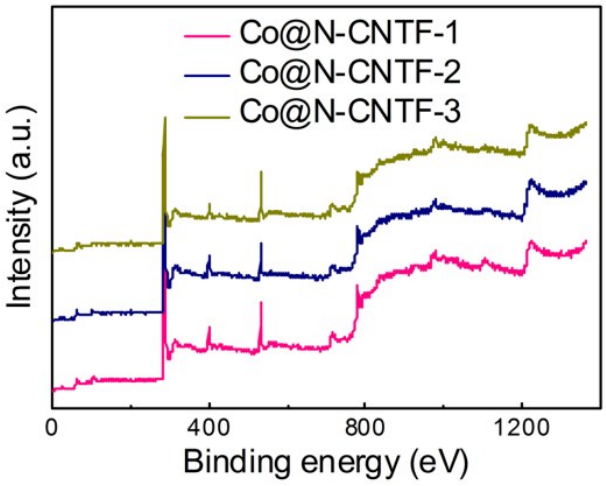

Fig. S5 XPS survey spectra of the Co@N-CNTF samples.

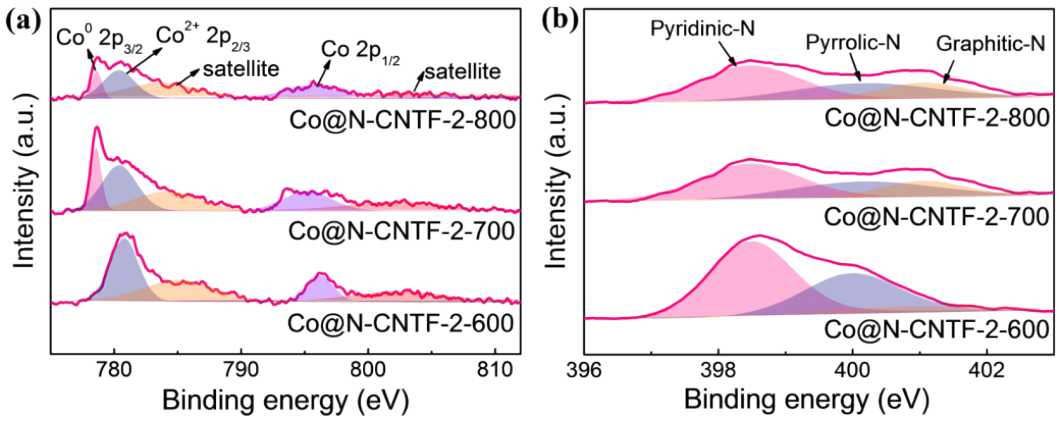

Fig. S6 (a) Co 2p and (b) N 1s XPS curves of the Co@N-CNTF-2-600, Co@N-CNTF-2-700 and Co@N-CNTF-2-800.

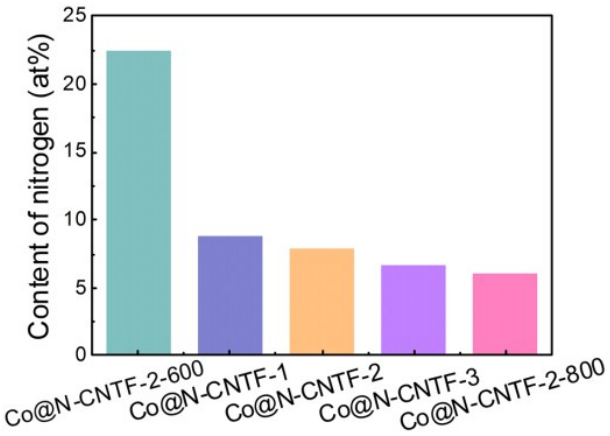

Fig. S7 Atomic contents of nitrogen in the Co@N-CNTF samples

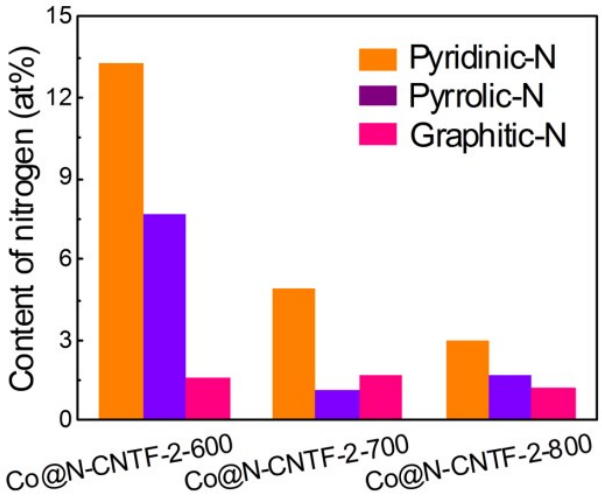

Fig. S8 Atomic contents of various nitrogen forms in the Co@N-CNTF-2-600, Co@N-CNTF-2-700 and Co@N-CNTF-2-800.

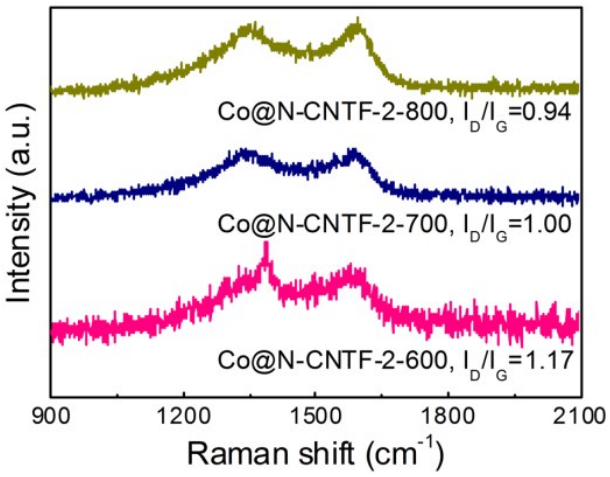

Fig. S9 Raman spectra of the Co@N-CNTF-2-600, Co@N-CNTF-2-700 and Co@N-CNTF-2-800.

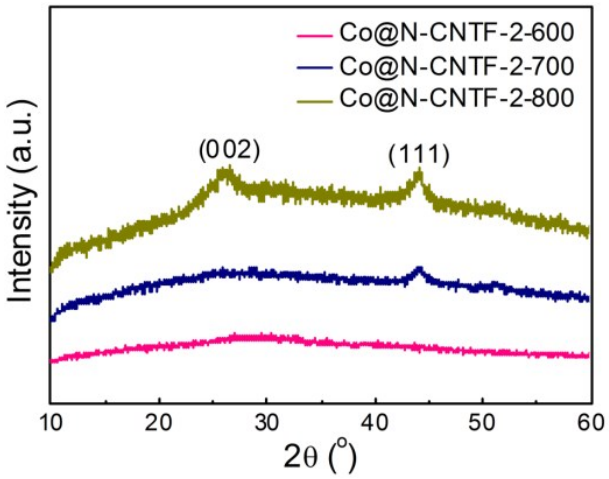

Fig. S10 XRD patterns of the Co@N-CNTF-2-600, Co@N-CNTF-2-700 and Co@N-CNTF-2-800.

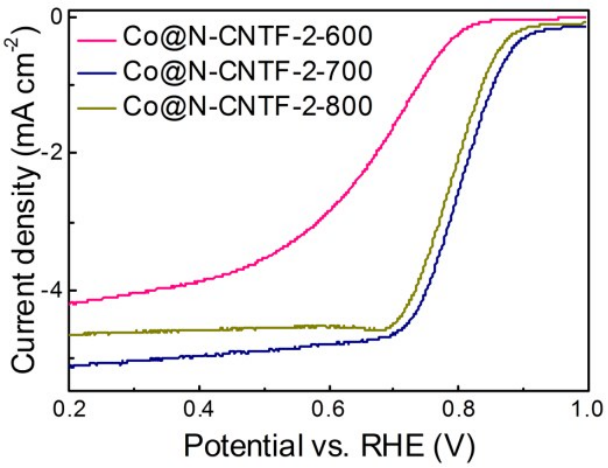

Fig. S11 LSV curves of the Co@N-CNTF-2-600, Co@N-CNTF-2-700 and Co@N-CNTF-2-800 in O_2-saturated 0.1 M KOH at 1600 rpm.

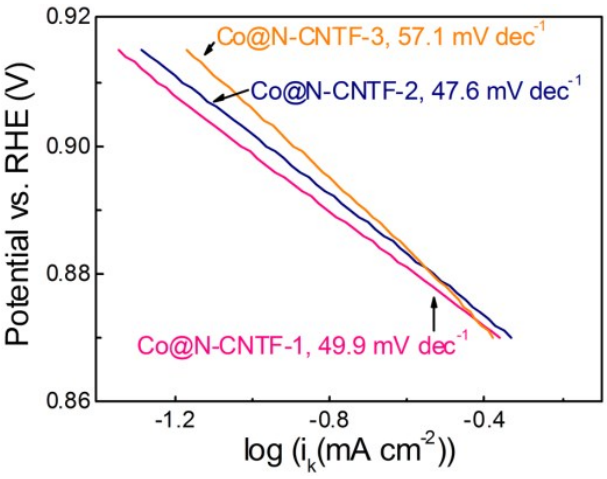

Fig. S12 Tafel slopes of the Co@N-CNTF-1, Co@N-CNTF-2 and Co@N-CNTF-3 in O_2-saturated 0.1 M KOH at 1600 rpm.

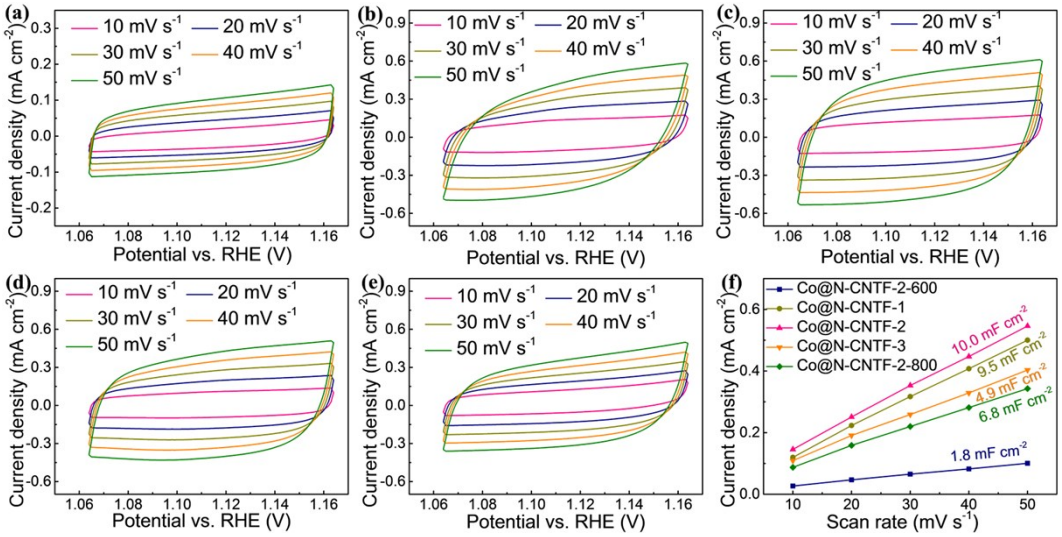

Fig. S13 CV plots of (a) Co@N-CNTF-2-600, (b) Co@N-CNTF-1, (c) Co@N-CNTF-2, (d) Co@N-CNTF-3, (e) Co@N-CNTF-2-800 at different scan rates. (f) The measured capacitive currents plotted as a function of scan rates.

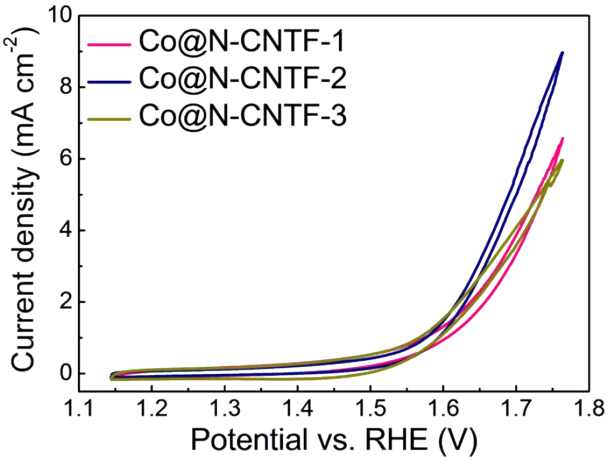

Fig. S14 CV curves of Co@N-CNTF-1, Co@N-CNTF-2 and Co@N-CNTF-3 in O_2-saturated 1 M KOH with a sweep rate of 5 mV s^{-1}.

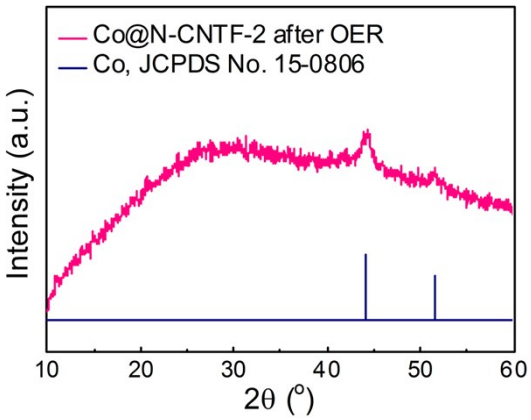

Fig. S15 XRD pattern of the Co@N-CNTF-2-700 after cycling for the OER.

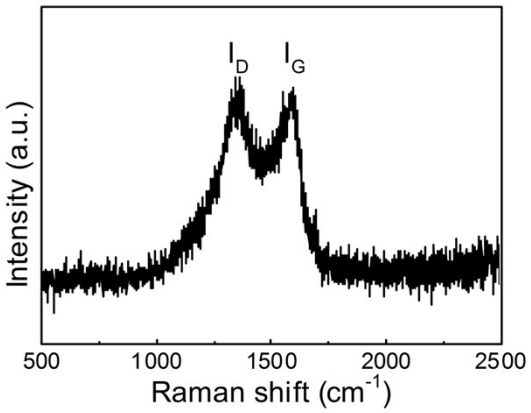

Fig. S16 Raman spectra of the Co@N-CNTF-2-700 after cycling for the OER.

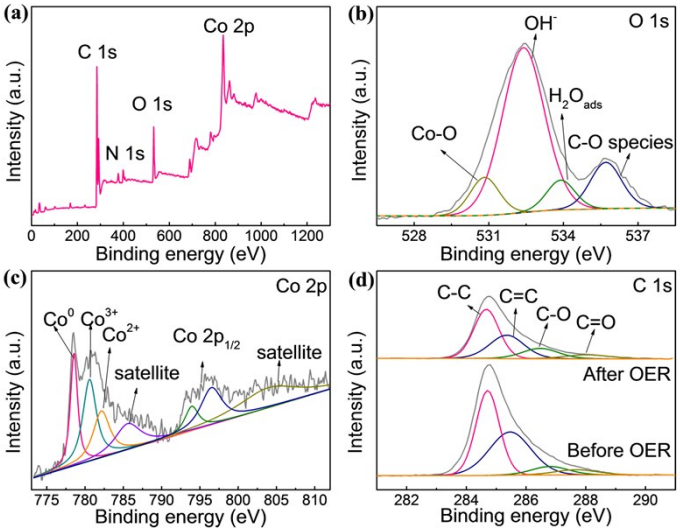

Fig. S17 XPS spectra of the Co@N-CNTF-2-700 after cycling for the OER. (a) XPS survey, (b) Co 2p, (c) O 1s, and (d) C 1s spectra.

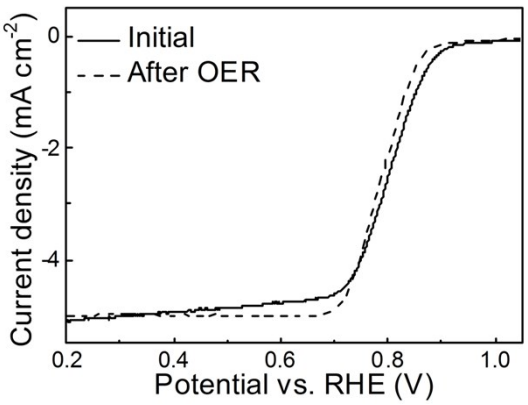

Fig. S18 The ORR performance of the Co@N-CNTF-2-700 after cycling for the OER.

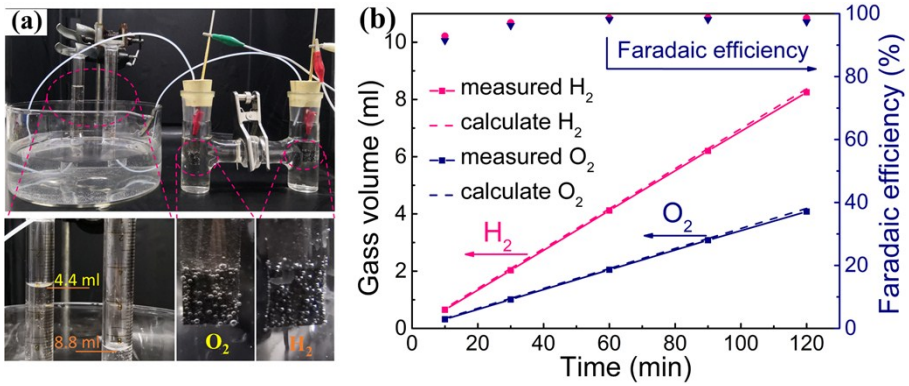

Fig. S19 Schematic of a home-made water splitting device using carbon cloth-loaded Co@N-CNTF-2 as both cathode and anode by chronopotentiometry at 10 mA cm^{-2}. (b) The volume of produced H_2 and O_2 as a function of the water-splitting time for the device.

Table 1. Summary of the ORR and OER activities of our Co@N-CNTF-2 catalysts with other Co-based bifunctional oxygen electrocatalysts in the literature.

Catalysts	$E_{1/2}$ (V vs. RHE)	$E_{j=10}$ (V vs. RHE)	ΔE (V vs. RHE)	Ref.
$Co@Co_3O_4/NC$	0.80	1.65	0.85	[1]
CoO@N/S-CNF	0.72	1.55	0.83	[2]
Co-PDA-C	0.77	1.60	0.83	[3]
Co_3O_4/NBGHSs	0.86	1.71	0.85	[4]
CoS_2/N,S-GO	0.79	1.61	0.82	[5]
CoO/N-G	0.81	1.57	0.76	[6]
Co-N/C 800	0.76	1.74	0.98	[7]
Co-NC-700	0.84	1.62	0.78	[8]
Co_3O_4@NPGC	0.84	1.68	0.84	[9]
Co@N-CNTF-2	0.81	1.63	0.77	**This work**

References

[1] A. Aijaz, J. Masa, C. Rosler, W. Xia, P. Weide, A. J. Botz, R. A. Fischer, W. Schuhmann and M. Muhler, *Angew. Chem. Int. Ed.*, 2016, **55**, 4087.

[2] T. Liu, Y.-F. Guo, Y.-M. Yan, F. Wang, C. Deng, D. Rooney and K.-N. Sun, *Carbon*, 2016, **106**, 84.

[3] B. Li, Y. Chen, X. Ge, J. Chai, X. Zhang, T. S. Hor, G. Du, Z. Liu, H. Zhang and Y. Zong, *Nanoscale*, 2016, **8**, 5067.

[4] T. Y. Ma, S. Dai, M. Jaroniec and S. Z. Qiao, *J Am Chem Soc* **2014**, *136*, 13925.

[5] Z. Jiang, Z.-J. Jiang, T. Maiyalagan and A. Manthiram, *J. Mater. Chem. A*, 2016, **4**, 5877.

[6] S. Mao, Z. Wen, T. Huang, Y. Hou and J. Chen, *Energy Environ. Sci.*, 2014, **7**, 609.

[7] W. Hu, Q. Wang, S. Wu and Y. Huang, *J. Mater. Chem. A*, 2016, **4**, 16920.

[8] B. Chen, X. He, F. Yin, H. Wang, D.-J. Liu, R. Shi, J. Chen and H. Yin, *Adv. Funct. Mater.*, 2017, **27**, 1700795.

[9] G. Li, X. Wang, J. Fu, J. Li, M. G. Park, Y. Zhang, G. Lui and Z. Chen, *Angew. Chem. Int. Ed.*, 2016, **55**, 4977.